INFLUENCE OF A SMALL AMOUNT OF TETHERED CHAINS ON WETTING TRANSITIONS: A DENSITY FUNCTIONAL APPROACH

Małgorzata BORÓWKO[1], Andrzej PATRYKIEJEW[2], Stefan SOKOŁOWSKI[3,*] and Tomasz STASZEWSKI[4]

Department for the Modeling of Physico-Chemical Processes, Maria Curie-Skłodowska University, 20-031 Lublin, Poland; e-mail: [1] borowko@hektor.umcs.lublin.pl, [2] andrzej@pluto.umcs.lublin.pl, [3] stefan@ork.umcs.lublin.pl, [4] tomo@heksan.umcs.lublin.pl

Received August 19, 2009
Accepted October 6, 2009
Published online February 25, 2010

Dedicated to Professor Ivo Nezbeda on the occasion of his 65th birthday.

A density functional approach to adsorption and phase behavior of a simple fluid from gas phase on a surface modified with a small amount of grafted chains is presented. The chains are modeled as freely jointed tangent spheres with end segments attached to the surface. The segments and gas molecules interact via the Lennard–Jones potential. We have found that the presence of preadsorbed chains considerably affects wettability of solid surfaces. An increase in the amount of grafted chains leads to a crossover between prewetting and layering transitions. This crossover occurs by merging of successive layering transitions.
Keywords: Density functional theory; Phase transitions; Thin films; Thermodynamics.

Substances obtained by attachment of chain molecules to solid surfaces play an important role in several technological processes. In particular, surface modification is used as a method of stabilization of colloidal suspensions, a method for development of protective films and adhesives, and so forth[1–4]. The adsorbents covered by chemically bonded polymers are also used as stationary phases in gas chromatography and reversed-phase liquid chromatography. In fact, the reversed-phase liquid chromatography constitutes now one of the most important separation techniques[5]. Its further improvement requires detailed understanding of adsorption and separation processes at molecular level[6].

Different theoretical approaches were used to describe adsorption of gases on solid surfaces modified by tethered chains. One of the first treatments of tethered chains was proposed by Alexander[7] and de Gennes[8]. The description of such systems was greatly improved by Milner, Written and Cates[9,10]

Collect. Czech. Chem. Commun. 2010, Vol. 75, No. 2, pp. 221–241

doi:10.1135/cccc2009104

who presented self-consistent field equations for stretched polymer brushes in a good solvent. The self-consistent field theory was then employed by numerous authors[11–16]. A further progress in theoretical studies resulted from application of the single-chain mean-field method[17–19], according to which the statistical mechanics of a single chain is treated exactly, whereas the interaction with other chains is taken into account at a mean-field level.

In the last decade several versions of the density functional approach were applied in description of the end-grafted chains. McCoy and co-workers[18,20–22] and Wu et al.[23–25] considered the behavior of chains in an implicit solvent as well as in a "continuum solvent approximation". Also, other versions of density functional theory were developed[26–28].

Recently, the Yu–Wu[23,24,29–31] density functional theory was applied in description of adsorption of hard-sphere mixtures[32,33] and a one-component Lennard–Jones fluid[34] on surfaces modified by preadsorbed chain molecules. Theoretical studies of the systems of interest were supplemented by numerous computer simulations[35–45]. A significant aim of many simulations was to explain the mechanism of structural transitions in surface films.

In our previous works[32–34] we proposed and tested theoretical tools to study adsorption on surfaces modified with brush-like structures formed by preadsorbed chains. The theory was based on the development of Yu and Wu[29,31,46,47] and was proven[32,33] to correctly reproduce computer simulation data of adsorption of hard spheres and their mixtures on surfaces modified with tethered hard-sphere chains. This theory was also applied to a study of layering transitions[34]. We have demonstrated that the presence of tethered chains significantly influences layering transitions. However, our calculations concentrated on the study of surfaces covered with a dense layer of preadsorbed chains. The case of a sparse modifying layer as well as the question how the presence of tethered chains influences wettability of solid surfaces has not been considered. Therefore, the aim of the present work is to study wetting properties of a surface covered with a small amount of grafted chains. In particular, we investigate a crossover between prewetting and layering transitions regimes.

Of course, the properties of the system and the picture of phase transitions depend on the choice of model parameters. The specific calculations presented below are carried out for a "minimal" model, i.e. for a model in which the number of adjustable parameters has been reduced to minimum. The paper is organized as follows. First, we briefly outline the theory and

then in the following section we present the results of density functional calculations.

THEORY

The model we use is as follows[34]. Before adsorption, the adsorbent is prepared by binding a given amount of chain molecules to its surface. Each bonded chain consists of M tangentially linked spherical segments of the same diameter $\sigma^{(C)}$. The terminating segment, $j = 1$, of each chain is bonded to the surface, i.e. its local density is given by

$$\rho_{s,1}^{(C)}(z) = \mathcal{C}\delta(z - \sigma^{(C)}/2) \tag{1}$$

where the normalization constant, $\mathcal{C}$, is calculated from the imposed constraint of a constancy of the number of tethered chains per unit surface area

$$\rho_C = \int \mathrm{d}z\, \rho_{s,1}^{(C)}(z) \tag{2}$$

where z is a distance from the surface. The energy of interaction of all remaining segments, $j = 2, \ldots, M$, with the surface is

$$v_j^{(C)}(z) = \begin{cases} \infty & \text{for } z < \sigma^{(C)}/2 \\ 0 & \text{otherwise} \end{cases} . \tag{3}$$

The connectivity of a chain is ensured by the bonding potential between two adjacent segments, v_b. The total bonding potential satisfies the relation[29]

$$\exp[-\beta V_b(\mathbf{R})] = \prod_{i=1}^{M-1} \delta(|\mathbf{r}_{i+1} - \mathbf{r}_i| - \sigma^{(C)}) / 4\pi(\sigma^{(C)})^2 \tag{4}$$

where $\mathbf{R} \equiv (\mathbf{r}_1, \mathbf{r}_2, \ldots, \mathbf{r}_M)$ denotes a set of coordinates describing the segment positions.

After preparation of the surface we perform adsorption of Lennard–Jones species, S, of diameter $\sigma^{(S)}$. This process takes place from a reservoir containing one-component fluid at a fixed chemical potential μ. Obviously, the adsorption influences the structure of the preadsorbed layer of chains, but cannot change their amount.

The spherical molecules of a fluid interact with the surface via Lennard–Jones (9–3) potential

$$v^{(S)}(z) = \varepsilon_{gs}[(z_0 / z)^9 - (z_0 / z)^3]. \quad (5)$$

Moreover, all spherical species (i.e., segments and fluid particles) interact via the Lennard–Jones (12–6) potentials, $u^{(ij)}(r)$, $i, j = S, C$,

$$u^{(ij)}(r) = 4\varepsilon^{(ij)}[(\sigma^{(ij)} / r)^{12} - (\sigma^{(ij)} / r)^6] \quad \text{for} \quad r \le r_{\text{cut}}^{(ij)} \quad (6)$$

where $r_{\text{cut}}^{(ij)}$ is the cut-off distance. We assume additivity of the diameters as common, i.e. $\sigma^{(ij)} = (\sigma^{(i)} + \sigma^{(j)})/2$, $i, j = C, S$.

The structure of fluid is described by the local density of fluid particles, $\rho^{(S)}(z)$, and the local densities of segments, $\rho_{s,j}^{(C)}(z)$. Of course,

$$\rho_{s,j}^{(C)}(\mathbf{r}) = \int d\mathbf{R}\, \delta(\mathbf{r} - \mathbf{r}_j)\, \rho^{(C)}(\mathbf{R}) \quad (7)$$

where $\rho^{(C)}(\mathbf{R})$ is the local density of chains, which is a function of the coordinates of all the segments. We also introduce the total segment density as

$$\rho_s^{(C)}(\mathbf{r}) = \sum_{j=1}^{M} \rho_{s,j}^{(C)}(\mathbf{r}). \quad (8)$$

The density functional theory for the model formulated above was reported in our previous works[32–34]. Briefly, we use the grand canonical ensemble with the constraint (*2*). The thermodynamic potential reads

$$\Omega = F[\rho^{(C)}(\mathbf{R}), \rho^{(S)}(\mathbf{r})] + \int d\mathbf{R}\, \rho^{(S)}(\mathbf{r})(v^{(S)}(\mathbf{r}) - \mu) \quad (9)$$

where $F[\rho^{(C)}(\mathbf{R}), \rho^{(S)}(\mathbf{r})]$ is the Helmholtz energy functional, which is divided into ideal term, F_{id}, and the excess term, F_{ex}, the latter due to the hard-sphere contribution, (hs), due to connectivity of chain molecules, (c), and due to attractive interactions between all spherical species, (att), $F = F_{\text{id}} + F_{\text{ex}}$, $F_{\text{ex}} = F_{\text{hs}} + F_{\text{c}} + F_{\text{att}}$. The configurational ideal part of the Helmholtz energy functional, F_{id} is[29]

$$\beta F_{\mathrm{id}} = \beta \int \mathrm{d}\mathbf{R}\, \rho^{(C)}(\mathbf{R})(V_{\mathrm{b}}(\mathbf{R}) +$$

$$+ \int \mathrm{d}\mathbf{R}\, \rho^{(C)}(\mathbf{R})[\ln(\rho^{(C)}(\mathbf{R}) - 1] + \int \mathrm{d}\mathbf{r}\, \rho^{(S)}(\mathbf{r})[\ln(\rho^{(S)}(\mathbf{r})) - 1]. \qquad (10)$$

The excess Helmholtz energy due to hard-sphere interactions results from the fundamental measure theory[29,30,48,49]

$$F_{\mathrm{hs}} = \int \Phi_{\mathrm{hs}}(\mathbf{r})\, \mathrm{d}\mathbf{r} \qquad (11)$$

where

$$\Phi_{\mathrm{hs}} = -n_0 \ln(1 - n_3) +$$

$$+ \frac{n_1 n_2 - \mathbf{n}_1 \cdot \mathbf{n}_2}{1 - n_3} + n_2^3 (1 - \xi^2)^3 \frac{n_3 + (1 - n_3)^2 \ln(1 - n_3)}{36\pi n_3^2 (1 - n_3)^2}. \qquad (12)$$

In the above $\xi(\mathbf{r}) = |\mathbf{n}_2(\mathbf{r})|/n_2(\mathbf{r})$. The scalar, n_α, for $\alpha = 0, 1, 2, 3$ and vector, $\mathbf{n}_\alpha$, for $\alpha = 1, 2$ weighted densities are given by

$$n_\alpha(\mathbf{r}) = n_\alpha^{(C)}(\mathbf{r}) + n_\alpha^{(S)}(\mathbf{r}) =$$

$$= \int \mathrm{d}\mathbf{r}' \rho_s^{(C)}(\mathbf{r}') w_\alpha^{(C)}(\mathbf{r} - \mathbf{r}') + \int \mathrm{d}\mathbf{r}' \rho_s^{(S)}(\mathbf{r}')\, w_\alpha^{(S)}(\mathbf{r} - \mathbf{r}') \qquad (13)$$

and

$$\mathbf{n}_\alpha(\mathbf{r}) = \mathbf{n}_\alpha^{(C)}(\mathbf{r}) + \mathbf{n}_\alpha^{(S)}(\mathbf{r}) =$$

$$= \int \mathrm{d}\mathbf{r}' \rho_s^{(C)}(\mathbf{r}') \mathbf{w}_\alpha^{(C)}(\mathbf{r} - \mathbf{r}') + \int \mathrm{d}\mathbf{r}' \rho_s^{(S)}(\mathbf{r}')\, \mathbf{w}_\alpha^{(S)}(\mathbf{r} - \mathbf{r}'). \qquad (14)$$

For the definitions of the weight functions $w_\alpha^{(i)}$ and $\mathbf{w}_\alpha^{(i)}$ see refs[30,48,49].

The contribution $F_{\mathrm{c}} = \int \Phi_{\mathrm{c}}(\mathbf{r})\, \mathrm{d}\mathbf{r}$, is evaluated from

$$\Phi_{(\mathrm{c})} = \frac{1 - M}{M} n_0^{(C)} \xi^{(C)} \ln[y_{(\mathrm{hs})}^{(C)}(\sigma^{(C)})] \qquad (15)$$

where $\zeta^{(C)} = 1 - \mathbf{n}_2^{(C)} \cdot \mathbf{n}_2^{(C)} / (n_2^{(C)})^2$, with $y_{(\mathrm{hs})}^{(C)}$ given by the Boublik–Mansoori–Carnahan–Starling–Leland[50,51] expression for the contact value of the radial

distribution function of spherical segments C in a mixture of hard spheres containing C and of S spheres

$$y^{(C)}_{(\mathrm{hs})}(\sigma^{(C)}) = \frac{1}{1-n_3} + \frac{n_2\sigma^{(C)}\zeta}{4(1-n_3)^2} + \frac{(n_2\sigma^{(C)})^2\zeta}{72(1-n_3)^3} \tag{16}$$

with $\zeta = 1 - \mathbf{n}_2 \cdot \mathbf{n}_2/(n_2)^2$.

Finally, the attractive force contribution results from the mean-field approximation applied to the attractive interactions between all the spherical segments

$$F_{\mathrm{att}} = \frac{1}{2}\sum_{i,j=S,C}\int \mathrm{d}\mathbf{r}\,\mathrm{d}\mathbf{r}'\rho_s^{(i)}(\mathbf{r})\rho_s^{(j)}(\mathbf{r}')u_{\mathrm{att}}^{(ij)}(|\mathbf{r}-\mathbf{r}'|) \tag{17}$$

where $u_{\mathrm{att}}^{(ij)}(|\mathbf{r}-\mathbf{r}'|)$ is the attractive part of the Lennard–Jones potential, defined according to the Weeks–Chandler–Andersen scheme[52]

$$u_{\mathrm{att}}^{(ij)}(r) = \begin{cases} \varepsilon^{(ij)} & r \le 2^{1/6}\sigma^{(ij)} \\ u^{(ij)}(r) & r > 2^{1/6}\sigma^{(ij)} \end{cases} \tag{18}$$

and the effective hard-sphere diameter is set to be $d^{(\mathrm{i})} = \sigma^{(\mathrm{i})}$, $i = S,C$.

The equilibrium structure of chains and of spherical particles is calculated minimizing $\mathcal{Y}$ under the constraint (*2*). Using the technique described in previous works[32–34] the density profiles are calculated from

$$\rho^{(S)}(z) = \exp[\beta\mu - \beta\lambda_1^{(S)}(z)] \tag{19}$$

and

$$\rho_{s,i}^{(C)}(z) = \tilde{C}\exp[-\beta\lambda_i(z)]G_i^{(L)}(z)G_{M+1-i}^{(R)}(z) \tag{20}$$

where $\lambda_j^{(i)}(z_j)$ are given as

$$\lambda_j^{(C)}(z_j) = \frac{\delta F_{\mathrm{ex}}}{\delta\rho_{\mathrm{s}}^{(C)}(z_j)} + v_j^{(C)}(z_j) \text{ for } j = 2, \ldots, M \text{ and } \lambda_1^{(S)}(z) = \frac{\delta F_{\mathrm{ex}}}{\delta\rho^{(S)}(z)} + v^{(S)}(z) \tag{21}$$

and where the functions $G_i^{(P)}(z)$, $P = L$, R are determined from the recurrence relations

$$G_i^{(L)}(z) = \int \mathrm{d}z' \exp[-\beta\lambda_{i-1}^{(C)}(z)] \frac{\theta(\sigma^{(C)} - |z - z'|)}{2\sigma^{(C)}} G_{i-1}^{(L)}(z') \qquad (22)$$

and

$$G_i^{(R)}(z) = \int \mathrm{d}z' \exp[-\beta\lambda_{M-i+2}^{(C)}(z)] \frac{\theta(\sigma^{(C)} - |z - z'|)}{2\sigma^{(C)}} G_{i-1}^{(L)}(z') \qquad (23)$$

for $i = 2, 3, \ldots, M$ and with $G_1^{(L)}(z) = G_1^{(R)}(z) \equiv 1$. We recall that the constant $\tilde{C}$ is evaluated from Eq. (*2*) which applies to any segment density profile $\rho_{s,j}^{(C)}(z)$. To complete the theory we write down equations defining the configurational chemical potential μ in terms of the bulk density ρ_b of spherical particles

$$\beta\mu = \ln\rho_b + \beta\mu_{(hs)} + \beta\rho_b \int u_{att}^{(SS)}(r)\,\mathrm{d}\mathbf{r} \qquad (24)$$

where $\mu_{(hs)}$ is the excess chemical potential of pure hard-sphere fluid at the density ρ_b resulting from the Boublik–Mansoori–Carnahan–Starling–Leland equation of state[50,51].

The excess adsorption isotherms are obtained from the following standard equation

$$\Gamma = \int \mathrm{d}z[\rho^{(S)}(z) - \rho_b]. \qquad (25)$$

RESULTS AND DISCUSSION

The principal aim of our calculations is to study the influence of a small amount of preadsorbed chains on adsorption of spherical molecules. In order to reduce the number of model parameters to a minimum, we have assumed equality of diameters and energy parameters of all spherical species, $\sigma^{(C)} = \sigma^{(S)} = \sigma$ and $\varepsilon^{(SS)} = \varepsilon^{(CS)} = \varepsilon^{(CC)} = \varepsilon$.

A common definition of the reduced temperature, $T^* = kT/\varepsilon$, is used. The diameter σ was used as the length unit. Therefore, the following reduced quantities are defined: the reduced distance from the surface $z^* = z/\sigma$, the reduced surface density $\rho_C^* = \rho_C/\rho_C\sigma^2$ and the reduced densities $\rho_b^* = \rho_b\sigma^3$, $\rho^{(S)*}(z) = \rho^{(S)}(z)\sigma^3$, $\rho^{(C)*}(z)_{s,j} = \rho_{s,j}^{(C)}(z)\sigma^3$, etc. Moreover, the reduced excess adsorption $\Gamma^* = \Gamma\sigma^2$ is used.

We assumed that $z_0 = 0.5\sigma$ in Eq. (*5*) and $r_{cut}^{(ij)} = 3.5\sigma$ in Eq. (*6*). The calculations were performed for the chains composed of $M = 5$ segments and the

energy parameter ε_{gs} equal to 8ε. Such a rather low value of ε_{gs} was selected to observe prewetting transition for a nonmodified surface.

We begin our discussion with the results obtained for a nonmodified surface, $\rho_C^* = 0$. Figure 1 shows examples of the adsorption isotherms calculated at lower (Fig. 1a) and higher (Fig. 1b) temperatures. At low temperatures the adsorption remains small up to the bulk liquid–vapor coexistence

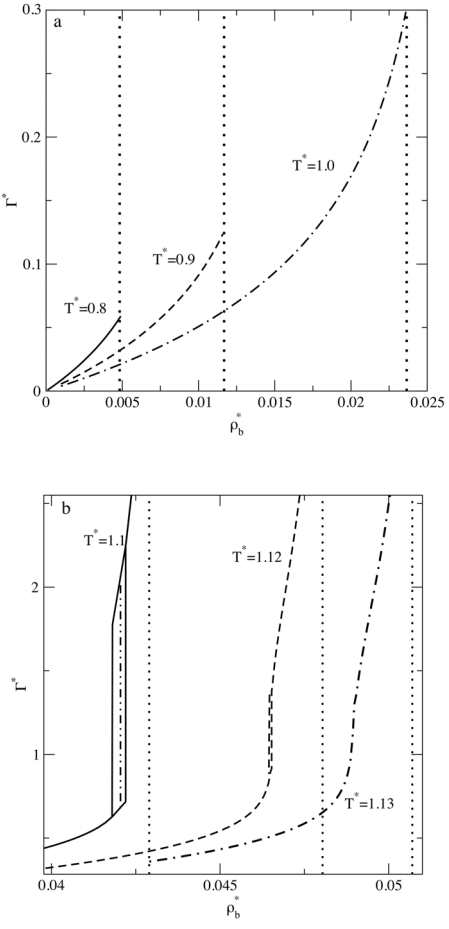

FIG. 1

A comparison of the adsorption isotherms on an unmodified surface, $\rho_C^* = 0$. Part a shows the isotherms at temperatures lower than the wetting temperature, part b at temperatures higher than the wetting temperature. Dotted vertical lines denote the bulk liquid–vapor transition densities. Part b shows the loops of hysteresis at two temperatures. The double dotted-dashed line denotes the equilibrium thin–thick film transition

density (the coexistence densities are marked here as vertical dotted lines). The isotherms displayed in Fig. 1a are characteristic for a situation when the liquid adsorbate does not wet the solid surface. As the temperature increases the picture of adsorption changes and for $T^* > 1.03$ we observe prewetting jumps on the isotherms and the adsorption diverges when ρ_b approaches the bulk liquid–vapor coexistence density. The prewetting jumps vanish at $T^* > 1.125$ and at these temperatures the adsorption grows continuously when ρ_b approaches its bulk coexistence value. Our calculations reveal that the unmodified system has the wetting temperature of $T_w^* \approx 1.03$, while the surface critical temperature is located at $T_{sc}^* \approx 1.025$.

The prewetting jump means that at a given temperature thin and thick adsorbed films coexist. This point is illustrated in Fig. 2, which shows the density profiles corresponding to the two coexisting adsorbed phases.

We now consider the case when a small amount of chains, with $\rho_C^* = 0.02$, has been deposited on the surface prior to adsorption of spherical species (quantitatively similar results have been observed even for $\rho_C^* = 0.01$). The preadsorbed chains significantly affect the adsorption of spherical species. Both characteristic temperatures, the wetting temperature and the surface critical temperature are shifted to much lower values; we have found that $T_w^* = 0.83$ and $T_{sc}^* = 0.92$. Examples of the adsorption isotherms are displayed in Fig. 3. At the temperatures $0.83 \leq T^* < 0.92$ we observe the existence of hysteresis loops. However, a closer inspection of the shape of ad-

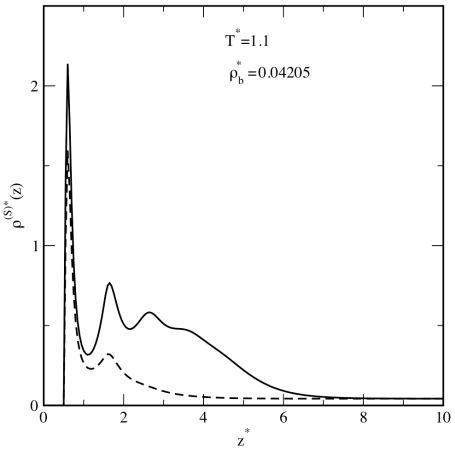

FIG. 2
The example of density profiles of thin (dashed line) and thick (solid line) films at $T^* = 1.1$ on an unmodified surface. The bulk density is given in the figure

sorption isotherms reveals a stepwise course of the curves. In particular, steps are clearly seen on the metastable part of the "desorption" branch at $T^* = 0.85$. At $T^* = 0.92$ the second step is continuous, but the first is discontinuous (although the relevant curve is not plotted here, we can say that at a slightly higher temperature $T^* = 0.925$, both steps are continuous. Therefore, we can state that the temperature 0.92 is only slightly lower than surface critical temperature). The steps observed on the isotherms can be treated as "precursors" of layering transitions in the system[53]. Thus we may expect that a further increase in the preadsorbed chain density should result in a change of the scenario of surface phase transitions.

Figure 4 demonstrates how the structure of the surface film at $T^* = 0.87$ changes with the bulk fluid density. Figure 4a illustrates the behavior of spherical molecules, whereas Fig. 4b shows the changes in the total segment density profiles, $\rho_s^{(C)}(z)$. The equilibrium prewetting transition at this temperature occurs at $\rho_b^* = 0.008655$. The dotted and long-dashed lines in Fig. 4a represent the profiles for thin and thick adsorbed films in equilibrium. At the fluid densities above the prewetting transition the film thickness grows and at the highest bulk density, $\rho_b^* = 0.00915$, it consists of almost nine filled layers. The first 5–6 layers exhibit well pronounced layered structure, but for the outer part of the adsorbed film a liquid-like plateau is observed.

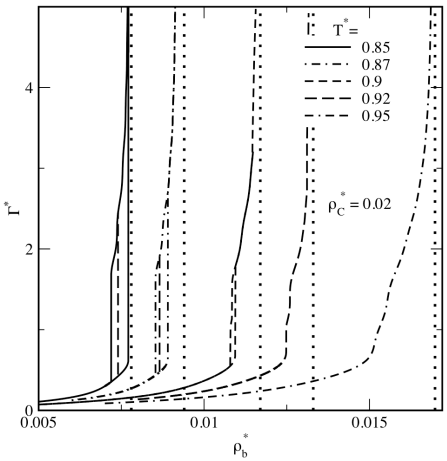

FIG. 3
Adsorption isotherms on a modified surface with $\rho_C^* = 0.2$ at the given temperatures. Dotted vertical lines denote the bulk liquid–vapor transition densities. At the two lowest temperatures, dashed vertical lines denote the equilibrium thin–thick film transition

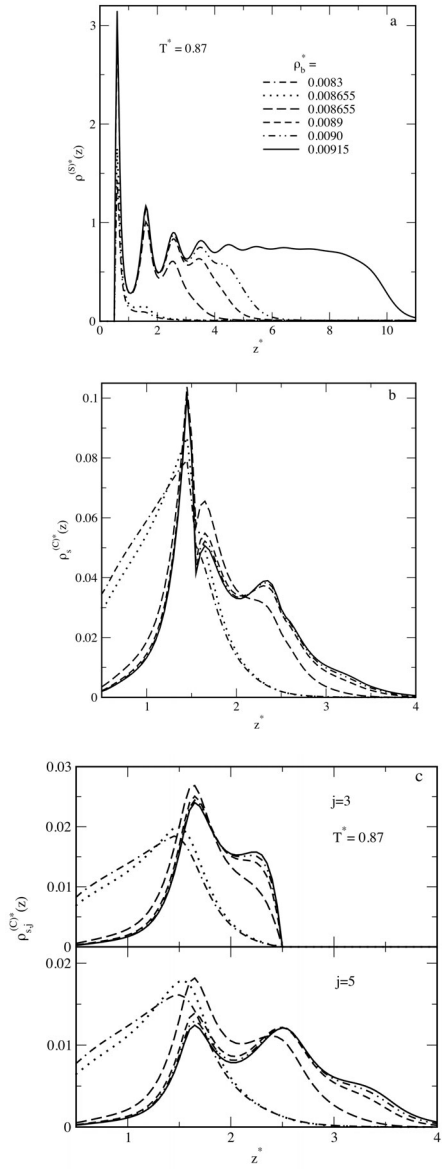

FIG. 4

The fluid density profiles (a), the total density profiles of segments (b) and individual segment density profiles of the middle (j = 3) and end (j = 5) segments (c). The calculations are for ρ_C^* = 0.2 at T^* = 0.87, and for the bulk fluid densities given in part a. The equilibrium prewetting transition occurs at ρ_b^* = 0.008655. In each part of the figure, we plotted two profiles corresponding to thin (short-dashed) and thick (long-dashed) fluid local densities

The changes in the structure of adsorbed fluid imply changes in the structure of tethered chains (see Fig. 4b). Note that the total segment density profiles shown in Fig. 4b are plotted for the distances $z^* > 0.5$, i.e. they do not include the profiles of the first segments, which are described by Eq. (*2*). For bulk fluid densities below the prewetting transition the chains are coiled, almost all segments occupy the space $z^* < 2$. The thin–thick film transition causes a rapid stretching-out of preadsorbed chains. This phenomenon is due to the "pushing" of segments of chains away from the surface by the fluid molecules forming a thick film and penetrating the space close to the surface. A further increase in the adsorbed film thickness results in a continuous, but rather small increase in stretching of the preadsorbed chains. To get a deeper insight into the changes in the structure of preadsorbed chains, in Fig. 4c we have presented the profiles of the middle ($j = 3$; upper panel) and the last ($j = 5$; lower panel) segments.

Figure 5 summarizes the results obtained so far. We show here the prewetting phase diagrams in the temperature–bulk fluid density plane (Fig. 5a) and in the temperature–chemical potential plane (Fig. 5b). In Fig. 5a, we show the diagrams evaluated for $\rho_C^* = 0$, 0.01 and 0.02, whereas in Fig. 5b only for $\rho_C^* = 0$ and 0.02. Each prewetting line starts at the bulk liquid–vapor coexistence at the wetting temperature and terminates at the surface critical temperature. As we have already noted, an increase in ρ_C^* results in lowering of both the wetting and surface critical temperatures.

A further increase in the preadsorbed chains density leads to qualitative changes in the phase behavior. Figure 6a shows the examples of adsorption isotherms obtained for $\rho_C^* = 0.05$ and at three different temperatures, $T^* = 0.725$, 0.75 and 0.775. In contrast to the previously considered cases, the isotherms show a number of steps. At the lowest temperature, $T^* = 0.725$, all these steps are discontinuous and exhibit van der Waals loops (for the sake of clarity, the lines corresponding to equilibrium transitions are not plotted). Each step is associated with the filling (adsorption branch) or emptying (desorption branch) of a consecutive layer, i.e. they depict a series of layering transitions. When the temperature increases, some of the discontinuous jumps are rounded off, but some of them survive. For example, at $T^* = 0.75$ the first layering transition, which corresponds to the filling of the layer adjacent to the solid surface, becomes continuous. Evidently, the critical temperature of this transition is lower than 0.75. However, the second, third and fourth transitions still exist. At higher temperatures the next layering transitions disappear and, instead discontinuous jumps, the isotherms consist of a series of continuous steps.

When the surface density of preadsorbed chains is slightly lowered to $\rho_C^* = 0.04$ (Fig. 6b) the scenario of phase transformations at higher temperatures is similar to that observed for $\rho_C^* = 0.05$. Clearly, the critical temperatures of particular layering transitions are different. However, at lower temperatures a qualitatively new behavior occurs. This point is illustrated in Fig. 6b, where adsorption isotherms at $T^* = 0.7$ on the surfaces characterized by $\rho_C^* = 0.05$ and 0.04 are presented. When $\rho_C^* = 0.05$, we observe well separated transitions associated with the filling of the first and second layer. For $\rho_C^* = 0.04$, the situation is different, the filling of the two first

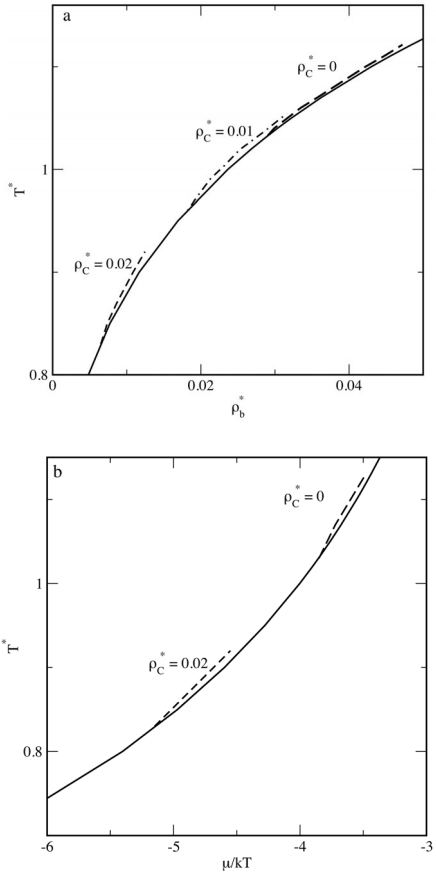

FIG. 5

Prewetting phase diagrams in the temperature–bulk fluid density (a) and the temperature–chemical potential (b) plane. The calculations are for $\rho_C^* = 0$, 0.01 and 0.02. The solid line denotes a part of the vapor branch of the bulk liquid–vapor diagram

layers occurs simultaneously. Moreover, also the van der Waals loop for the third transition is located very close to the transition described above. Thus one can suspect that at still lower temperatures the first, second and third layering transitions should merge. Unfortunately, because the density functional approach becomes less credible at low temperatures, the relevant calculations could not be carried out.

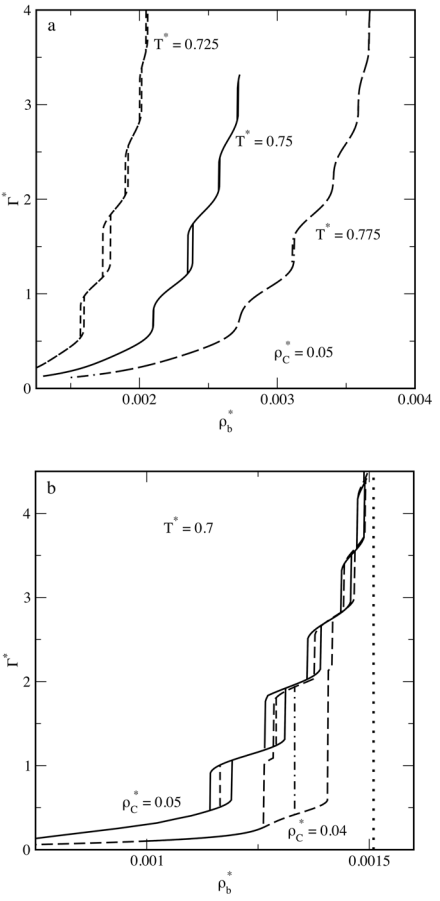

FIG. 6

The examples of adsorption isotherms exhibiting layering transitions, calculated for the modified surface with $\rho_C^* = 0.05$ (a) and a comparison of the isotherms on the surfaces of $\rho_C^* = 0.05$ and 0.04 at $T^* = 0.7$ (b). The dotted vertical line in part b marks the bulk liquid– vapor coexistence density, the dash-dotted line denotes the equilibrium transition associated with the filling the first two layers for the system of $\rho_C^* = 0.04$. For the system of $\rho_C^* = 0.05$, the first two layering transitions are marked by dashed vertical lines

Figure 7 shows the changes in the structure of the surface film resulting from the appearance of consecutive layering transitions. The results presented have been obtained for $\rho_C^* = 0.05$ and $T^* = 0.725$. The upper panel shows the fluid profiles, while the lower panel gives the total segment density profiles. Each layering transition results in the formation of one more adsorbed layer. The layers of adsorbed fluid influence the distribution of segments. The shapes of the displayed profiles indicate that with an increase in the amount of adsorbed fluid molecules the tethered chains become more and more stretched out.

Figure 8 summarizes the results for the modified surfaces with the surface densities of tethered chains $\rho_C^* = 0.05$ (Fig. 8a) and 0.04 (Fig. 8b). We have plotted here the phase diagrams corresponding to the first four layering transitions, together with a part of the bulk liquid–vapor phase diagram. Each of the layering transitions ends at the critical temperature. For $\rho_C^* = 0.04$, the critical temperatures of layering transitions decrease with a layer number: the critical temperature of the first transition is the highest, while that of the fourth transition is the lowest. However, for $\rho_C^* = 0.05$, the critical temperature changes in a nonmonotonic way: the highest critical temperature characterizes the transition connected with filling of the second layer. As we have already stressed while discussing the isotherms at $T^* = 0.7$ (Fig. 7, lower panel), at lower temperatures the layering transitions within

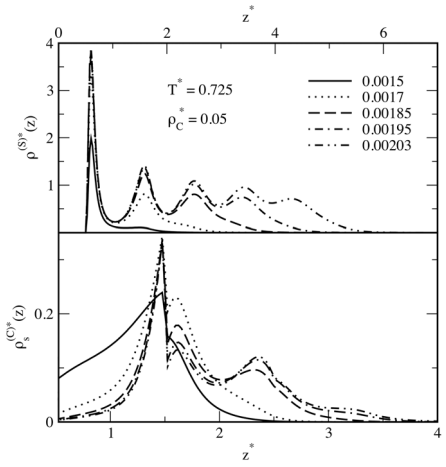

FIG. 7
Examples of density profiles corresponding to the filling of consecutive layers. Upper panel shows the fluid density profiles, lower panel shows the total segment density profiles. All the parameters are given in the figure

the first and second layers merge together. In other words, there must exist a triple point. Indeed, the triple point temperature (tt) is close to 0.71. Note that also the line for the third transition approaches the lines for the first and second transitions at low temperatures. Therefore, there should exist another triple point and at low temperatures the layering transition should be associated with the instantaneous filling the first three layers.

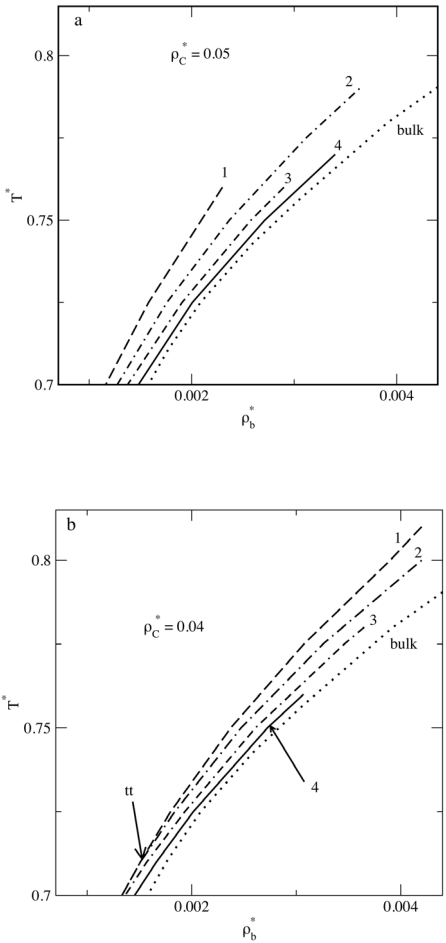

FIG. 8
Layering phase diagrams for the first four layering transitions. The layer numbers are given in the figure. The dotted line marked "bulk" is the vapor branch of the bulk liquid–vapor diagram. For $\rho_C^* = 0.05$ (a) and $\rho_C^* = 0.04$ (b). The triple point in part b is marked "tt"

Our calculations reveal two different scenarios of the phase transformations in the system. For very low values of ρ_C^*, we observe the prewetting (or a thin–thick film) transition. When ρ_C^* slightly increases, the prewetting transition transforms into a series of layering transitions. The low-temperature results ((Fig. 6b) for $\rho_C^* = 0.05$ and 0.04) suggest that the crossover between the two regimes results from the merging of a number of layering transitions.

To get a deeper insight into the crossover we have carried out the calculations for a lower value of $\rho_C^* = 0.03$.

In Fig. 9, we show an example of the isotherm at $T^* = 0.7$; this picture can be compared with Fig. 6b where the isotherms on the surfaces with $\rho_C^* = 0.05$ and 0.04 are presented. Similarly as for $\rho_C^* = 0.04$, the first layering transition is connected with the filling of two layers, but now the bulk density corresponding to the equilibrium third-layer filling is only slightly higher than the density of the first transition. Also, the bulk density for the next layering transition is close to the two previous ones. This means that the bulk densities for the consecutive layering transitions become closer and closer as ρ_C^* decreases from 0.05 to 0.03.

Figure 10 demonstrates the local density changes along the adsorption isotherm from Fig. 9. The upper panel displays the fluid density profiles, whereas the lower panel shows the total segment density profiles under the

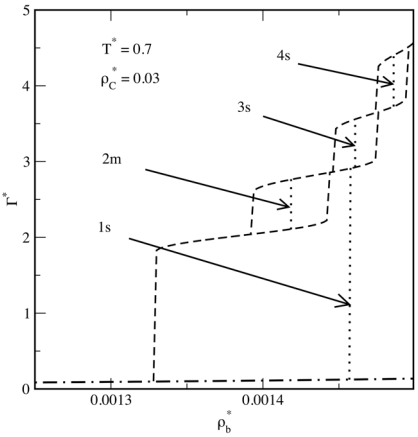

FIG. 9
The adsorption isotherm at $T^* = 0.7$ and for $\rho_C^* = 0.03$ exhibiting layering transitions. Dotted vertical lines denote the equilibrium transition densities that correspond to the same values of the thermodynamic potential $\mathcal{Y}$ for the coexisting phases. They are numbered 1–4. The labels "s" and "m" indicate thermodynamically stable and metastable transitions, respectively

same thermodynamic conditions. Let us discuss the fluid profiles at increasing bulk densities. The dotted line represents the profile well before the first transition occurs; the profile possesses one low peak located in the nearest vicinity of the wall. The next profile (dashed line) occurs just after the first transition (labeled in Fig. 9 as 1s), but before the consecutive transition (3s in Fig. 9). We can see that a film consisting of several layers has been developed. The third profile was evaluated at a bulk density slightly higher than that corresponding to the transition 3s in Fig. 9. The only change compared with the previous profile is that the last layer is now (almost) filled. As previously, the changes in the amount of adsorbed fluid cause changes in the distribution of chain segments and an increase in adsorption results in stretching out the chains.

A summary of the results for $\rho_C^* = 0.03$ is given in Fig. 11, where the phase diagram is shown. Comparing the diagram for $\rho_C^* = 0.03$ with that for $\rho_C^* = 0.04$, we can see that now all the curves for layering transitions plotted in Fig. 11 lie very close one to another. The triple point temperature is now much higher than that for the system of $\rho_C^* = 0.04$. Moreover, the auxiliary calculations have indicated that the triple point between the layering within the first two layers and that for the third layer is close to

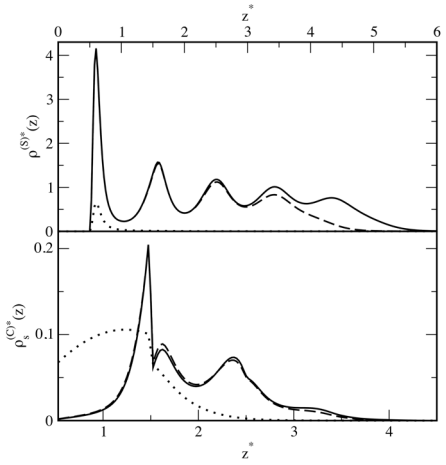

FIG. 10
Examples of density profiles corresponding to the filling of consecutive layers. The calculations were carried out for the system from Fig. 9. The upper panel shows the fluid density profiles, the lower panel gives the total segment density profiles. Dotted, dashed and solid lines were calculated at $\rho_C^* = 0.00135$, 0.001459 and 0.001464, respectively

0.695. However, the critical temperatures of the third and fourth transitions are similar for both systems of $\rho_C^* = 0.04$ and 0.03.

Let us summarize our observations: An increase in density of preadsorbed chains gives rise to qualitative changes in the phase behavior of the system. For $\rho_C^* \leq 0.02$, we can observe prewetting behavior, whereas for $\rho_C^* \geq 0.03$, layering transitions within the investigated temperature range. With increasing ρ_C^*, the relevant transition lines and their critical temperatures as well as the triple points shift towards lower temperatures. Within the considered approach the observed changes can be heuristically explained as follows. An increase in ρ_C^* results in an increase of the total attraction of the (modified) adsorbent–adsorbate interactions. We know that in the "strong adsorption (i.e. attraction) regime", a series of layerings occurs, whereas in the "intermediate adsorption regime", a prewetting behavior is expected. Our calculations have demonstrated that the crossover from layering to prewetting occurs via merging of layering transitions. In the beginning the first and second layerings flow together, next the third, and so on. In addition, the critical temperatures of higher layering transitions begin to be only weakly dependent on ρ_C^*, providing that ρ_C^* is low enough. The above described scenario leads to a transformation of layering transitions into a single prewetting transition when ρ_C^* decreases.

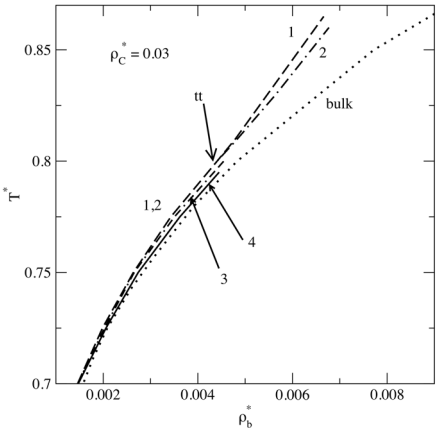

FIG. 11
Layering phase diagrams for the first four layering transitions for $\rho_C^* = 0.03$. The layer numbers are given in the figure. The dotted line marked "bulk" is the vapor branch of the bulk liquid–vapor diagram. The triple point is marked "tt"

It would be of interest to carry out more complete studies searching for an influence of different parameters, such as the intermolecular potential parameters, sizes of particles, and so on, on the phase behavior of the system. We hope to address these problems in future work.

This work was supported by the Ministry of Science of Poland (Grant No. N N204 123737).

REFERENCES

1. Netz R. R., Andelman D.: *Phys. Rep.* **2003**, *380*, 1.
2. Liakos I. L., Newman R. C., McAlpine E., Alexander M. R.: *Surf. Interface Anal.* **2004**, *36*, 347.
3. Weaver J. F., Carlsson A. F., Madix R. J.: *Surf. Sci. Rep.* **2003**, *50*, 107.
4. Charlaganov M., Koovan P., Leermakers F. A. M.: *Soft Matter* **2009**, *5*, 1448.
5. Neue U. D.: *HPLC Columns: Theory, Technology and Practice*. Wiley–Interscience, New York 1997.
6. Dorsey J. H., Dill K. A.: *Chem. Rev.* **1989**, *89*, 331.
7. Alexander S.: *J. Phys. (France)* **1977**, *38*, 983.
8. de Gennes P. G.: *Macromolecules* **1980**, *13*, 1069.
9. Milner S. T., Witten T. A., Cates M. E.: *Europhys. Lett.* **1988**, *5*, 413.
10. Milner S. T., Witten T. A., Cates M. E.: *Macromolecules* **1988**, *21*, 2610.
11. Zhulina E. B., Borisov O. V., Pryamitsyn V. A., Birshtein T. M.: *Macromolecules* **1991**, *24*, 140.
12. Patra C. N., Yethiray A., Curro J. G.: *J. Chem Phys.* **1999**, *111*, 1608.
13. Leermakers F. A. M., Philipsen H. J. A., Klumperman B.: *J. Chromatogr., A* **2002**, *959*, 37.
14. Stoyanov S. D., Paunov V. N., Rehage H., Kuhn H.: *Phys. Chem. Chem. Phys.* **2004**, *6*, 596.
15. Manciu M., Ruckenstein E.: *Langmuir* **2004**, *20*, 6490.
16. Pang P., Koska J., Coad B. R., Brooks D. E., Haynes C. A.: *Biotechnol. Bioeng.* **2005**, *90*, 1.
17. Carignano M. A., Szleifer I.: *J. Chem. Phys.* **1994**, *100*, 3210.
18. Szleifer I., Carignano M. A.: *Adv. Chem. Phys.* **1996**, *94*, 165.
19. Wang J., Müller M.: *Macromolecules* **2009**, *42*, 2251.
20. McCoy J. D., Ye Y., Curro J. G.: *J. Chem. Phys.* **2002**, *117*, 2975.
21. Ye Y., McCoy J. D., Curro J. G.: *J. Chem. Phys.* **2003**, *119*, 555.
22. McCoy J. D., Teixeira M. A., Curro J. G.: *J. Chem. Phys.* **2001**, *114*, 4289.
23. Cao D. P., Wu J.: *Langmuir* **2006**, *22*, 2712.
24. Jiang T., Li Z., Wu J. Z.: *Macromolecules* **2007**, *40*, 334.
25. Xu X., Cao D.: *J. Chem. Phys.* **2009**, *130*, 164901.
26. Frischknecht A. L.: *J. Chem. Phys.* **2008**, *128*, 224902.
27. Taniguchi T.: *J. Phys. Soc. Jpn.* **2009**, *78*, 041009.
28. Xu X., Cao D., Zhang X., Wang W.: *Phys. Rev. E* **2009**, *79*, 021805.
29. Yu Y. X., Wu J.: *J. Chem. Phys.* **2002**, *117*, 2368.
30. Yu Y. X., Wu J.: *J. Chem. Phys.* **2002**, *117*, 10165.
31. Yu Y. X., Wu J.: *J. Chem. Phys.* **2003**, *118*, 3835.
32. Borówko M., Rżysko W., Sokołowski S., Staszewski T.: *J. Chem Phys.* **2007**, *126*, 214703.

33. Borówko M., Rżysko W., Sokołowski S., Staszewski T.: *J. Phys. Chem. B* **2009**, *113*, 4763.
34. Patrykiejew A., Sokołowski S., Tscheliessnig R., Fischer J., Pizio O.: *J. Phys. Chem. B* **2008**, *112*, 4552.
35. Grest G. S., Murat M.: *Macromolecules* **1993**, *26*, 3108.
36. Lai P. Y., Binder K.: *J. Chem. Phys.* **1992**, *97*, 586.
37. Grest G. S.: *J. Chem. Phys.* **1996**, *105*, 5532.
38. Pastorino C., Binder K., Keer T., Mueller M.: *J. Chem. Phys.* **2006**, *124*, 064902.
39. Ohno K., Sakamoto T., Minagawa T., Okabe Y.: *Macromolecules* **2007**, *40*, 723.
40. Descas R., Sommer J. U., Blumen A.: *J. Chem. Phys.* **2006**, *125*, 214702.
41. Patra M., Linse P.: *Nano Lett.* **2006**, *6*, 133.
42. MacDowell L. G., Mueller M.: *J. Chem. Phys.* **2006**, *124*, 084907.
43. Lippa K. A., Sander L. C., Mountain R. D.: *Anal. Chem.* **2005**, *77*, 7862.
44. Rafferty J. L., Siepmann J. I., Schure M. R.: *J. Chromatogr., A* **2008**, *1204*, 11.
45. Rafferty J. L., Siepmann J. I., Schure M. R.: *J. Chromatogr., A* **2008**, *1204*, 20.
46. Fu D., Wu J.: *Ind. Eng. Chem. Res.* **2005**, *44*, 1120.
47. Wu J., Li Z.: *Annu. Rev. Phys. Chem.* **2007**, *58*, 85.
48. Rosenfeld Y.: *Phys. Rev. Lett.* **1989**, *63*, 980.
49. Roth R., Evans R., Lang A., Kahl G.: *J. Phys. Condens. Matter* **2002**, *14*, 12063.
50. Boublik T.: *J. Chem. Phys.* **1970**, *53*, 471.
51. Mansoori G. A., Carnahan N. F., Starling K. E., Leland T. W.: *J. Chem. Phys.* **1971**, *54*, 1523.
52. Weeks J. D., Chandler D., Andersen H. C.: *J. Chem. Phys.* **1971**, *54*, 5237.
53. Pandit R., Schick M., Wortis M.: *Phys. Rev. B* **1982**, *26*, 5112.